

NMR-Based Determination of the 3D Structure of the Ligand–Protein Interaction Site without Protein Resonance Assignment

Julien Orts,^{*,†} Marielle Aulikki Wälti,[†] May Marsh,[‡] Laura Vera,[‡] Alvar D. Gossert,[§] Peter Güntert,^{†,||} and Roland Riek^{*,†}

[†]ETH Zürich, Laboratory of Physical Chemistry, HCI F217, Vladimir-Prelog-Weg 2, 8093 Zürich, Switzerland

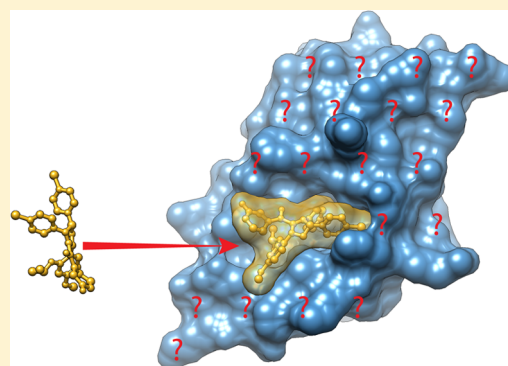
[‡]Swiss Light Source, Paul Scherrer Institute, CH-5232 Villigen, Switzerland

[§]Novartis Institutes for BioMedical Research, Novartis AG, CH-4002 Basel, Switzerland

^{||}Institute of Biophysical Chemistry, Center for Biomolecular Magnetic Resonance, and Frankfurt Institute of Advanced Studies, Goethe University Frankfurt am Main, Frankfurt am Main 60323, Germany

S Supporting Information

ABSTRACT: Molecular replacement in X-ray crystallography is the prime method for establishing structure–activity relationships of pharmaceutically relevant molecules. Such an approach is not available for NMR. Here, we establish a comparable method, called NMR molecular replacement (NMR^2). The method requires experimentally measured ligand intramolecular NOEs and ligand–protein intermolecular NOEs as well as a previously known receptor structure or model. Our findings demonstrate that NMR^2 may open a new avenue for the fast and robust determination of the interaction site of ligand–protein complexes at atomic resolution.



INTRODUCTION

X-ray crystallography molecular replacement (MR)¹ is a highly versatile tool for the detailed characterization of lead compounds and binding modes in the pharmaceutical industry.² The two major limitations of its application to drug research are (i) the availability of a similar protein structure and (ii) obtaining well-diffracting crystals of the ligand–protein complexes of interest. Although nowadays the first point is often not a limitation anymore, obtaining well-diffracting crystals can be difficult. In such situations, structure determination of protein–ligand complexes by liquid-state NMR appears to be an option. Unfortunately, the established standard structure determination protocol³ is in general time-consuming, and a shortcut using available structural data as in the case of MR in X-ray crystallography is not available. More recently, attempts to derive structures of protein–ligand complexes by NMR more efficiently have been proposed including the use of ambiguous distance restraints^{4,5} derived from nuclear Overhauser enhancements (NOEs), chemical shift perturbations,^{6–10} or saturation transfer experiments^{11,12} in combination with computational methods such as docking and scoring.^{13–16} (See Table S1 for a detailed comparison.) Here, we establish a MR-like approach in NMR called NMR molecular replacement (NMR^2) for the structure calculation of the binding pocket of ligands at atomic resolution bypassing protein resonance assignments. The method relies on the collection of assigned intraligand and not assigned semi-

quantitative intermolecular NOE distance restraints^{17–19} as well as on a known (homologous) protein structure. As we shall see, when applied to the cancer-relevant proteins HDMX, HDM2, and ABL,^{20,21} NMR^2 yielded the structures of protein–ligand interaction sites with high accuracy.

RESULTS AND DISCUSSION

The workflow of NMR^2 comprises six steps: (i) production of ¹³C,¹⁵N-labeled protein, (ii) sample preparation of ¹³C,¹⁵N-labeled protein with unlabeled ligand, (iii) measurements and analysis of F_1, F_2 -^{[15N,13C]-filtered [1H,1H]-spectra} for resonances assignment and structure calculation of the ligand,^{22–24} (iv) measurements and analysis of a series of F_1 -^{[15N,13C]-filtered [1H,1H]-NOESY experiments}^{22–25} with different mixing times for the collection of semiambiguous, semi-quantitative ligand–protein NOE restraints, (v) selection of an appropriate protein structure from the Protein Data Bank (PDB), including eventually the preparation of a homology model of the protein,²⁹ and (vi) multiple cycles of high-throughput series of structure calculations carried out by an in-house program using the CYANA software.³⁰ The restraints of step iv are of a semiambiguous nature because of the lack of a resonance assignment of the protein, they are between an

Received: November 26, 2015

Published: March 4, 2016

assigned proton of the ligand and an unassigned proton on the protein (Figure 1a). To reduce the ambiguity, a classification is

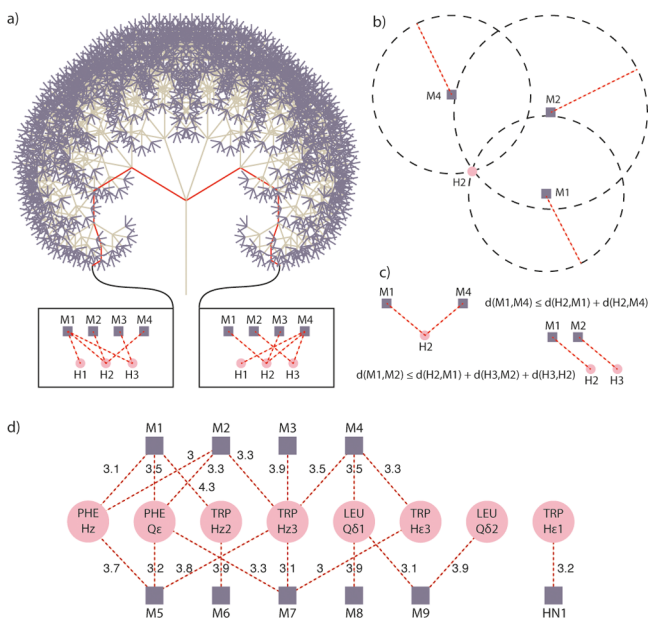


Figure 1. Key ideas of the NMR² method. (a) Tree of all possible distance combinations with 6 intermolecular NOEs connecting 4 unassigned methyl groups (M1–M4) to 3 assigned ligand protons (H1–H3). Two possible networks of intermolecular distance restraints (red dashed lines) are depicted within the boxes below the tree, each representing one path (red) on the tree. (b) Intersection of three distances define two possible positions of the proton H2 in a 3D space, both points defining a line perpendicular to the methyl's plane. (c) Graphical representation of the triangle and tetra-angle bounds smoothing inequalities, using three and four distances, respectively. (d) Experimentally derived distances depicted in dashed red lines with values in Å connecting ligand protons to methyl (M1–M9) or amide (HN1) groups.

made that evaluates on the basis of the ¹H chemical shift whether the unknown ¹H is from an amide or a methyl moiety. By following the previous formalism and the eNOE

protocol^{17,26–28} without spin diffusion correction, these restraints are semiquantitative.

This software package gradually includes the intermolecular distances, selects for the most promising intermediate structures, and discards the irrelevant ones after each cycle in order to keep the computation time requirement under control. The structure calculations are done with the protein structure obtained from step v, the ligand structure determined in step iii, and the intermolecular restraints from step iv, which for each subcalculation are assigned to one of the many possible assignments as outlined in Figure 1a (also below). The calculated structures with the smallest violations of the input restraints are selected to represent the protein–ligand complex (Figure S1). This protocol provides a fast and reliable determination of the interaction site structure because only a few days of measuring time and analysis are required.

Although the proposed protocol of NMR² appears straightforward, there is the major bottleneck of the number of structures to be calculated because of the ambiguity of the intermolecular restraints. Figure 1a highlights the tree of all possible distance combinations, 4⁶, of a simplified case with 6 intermolecular NOEs connecting 4 protein methyl groups with 3 ligand protons assigned. When applied to a real protein system such as the protein HDMX discussed below with 54 methyl groups and 10 intermolecular restraints, the number of possible combinations is very large (~10¹⁷) making it impossible to calculate structures for all possible assignments. However, bounds smoothing on the basis of the triangle and tetra-angle inequalities, which can be applied to any pair of intermolecular distance restraints (Figure 1c,b), decreases the amount of structures to be calculated significantly. In conjunction, a recursive algorithm that starts with a subset of selected distance restraints and gradually incorporates the others into the structure calculation allows a reduction of the number of structures to be calculated by more than 10 orders of magnitude (Table 1).

NMR² was applied to the oncoprotein HDMX^{20,21} in complex with the peptide-analogue Ac-Phe-Met-Aib-Pmp-6Cl,Trp-Glu-Ac3c-Leu-NH₂ (cmpd2, Figure S2b) using experimental data.³¹ First, the NOE-derived structure of cmpd2

Table 1. Summarized Results of Structure Calculations by NMR²

ligand–protein complex (PDB structure) ^a	flexibility ^b	reference structure ^c	first structure rmsd (Å) ^d	best rmsd (Å) ^e	distance restraints ^f	cycles ^g	true positives (%) ^h	calculations ⁱ
HDMX–cmpd2 (3fea, X-ray)	none	3fea	0.9	0.4	16	3	100	24868
HDMX–cmpd1 (3fe7, X-ray)	side chains	3fea	0.9	0.9	16	3	100	56659
HDM2–β-hairpin (2axi, X-ray)	side chains	3fea	1.1	1.0	21	5	100	82503
apo-HDM2 (1z1m, NMR)	full	3fea	1.8	1.8	21	9	30/60*	78632116
HDM2–nutlin-3a (3v3b, X-ray)	side chains	5c5a	0.9**	0.9**	16	5	100	17919188
HDM2–pip1 (4erf, X-ray)	side chains	2lzg (NMR)	1.5	1.5	23	6	100	1881884
HDM2–spiro (4lwt, X-ray)	none	4lwt	0.6**	0.6**	19†	2	100	857367
ABL–dasatinib (2gqg, X-ray)	side chains	2gqg	1.1	0.9	29†	9	100	4650907

^aThe PDB code with the method used for the structure determination is indicated in parentheses. ^bRegions with allowed flexibility of the protein in the structure calculations labeled with either “none” for a rigid protein, “side chains” for side chain flexibility, or “full” flexibility preserving the secondary structure elements by H-bond restraints. ^cPDB code of the reference protein–ligand complex structure. ^dHeavy atom rmsd of the best-ranked ligand structure computed after optimal superposition of the protein coordinates on the reference structure. ^eSimilarly, the smallest ligand rmsd to reference among the first 10 NMR² structures. **, The rmsd was calculated by excluding nutlin-3a moiety that points toward the solvent shown in Figure 4b and the heterocyclohexane for the spiroindolinone with voluntary erroneous conformation (Figure S10). ^fNumber of intermolecular distance restraints; † designates in silico restraints. ^gNumber of calculation cycles after each of which the amount of intermolecular distance restraints is increased and only a subset of the calculated structures is taken further in the process according to the criteria mentioned in the main text. ^hPercentage of NMR² structures with rmsd < 2 Å (*, rmsd < 4.5 Å) among the 10 final structures. ⁱTotal number of structure calculations with different assignments of the intermolecular distance restraints.

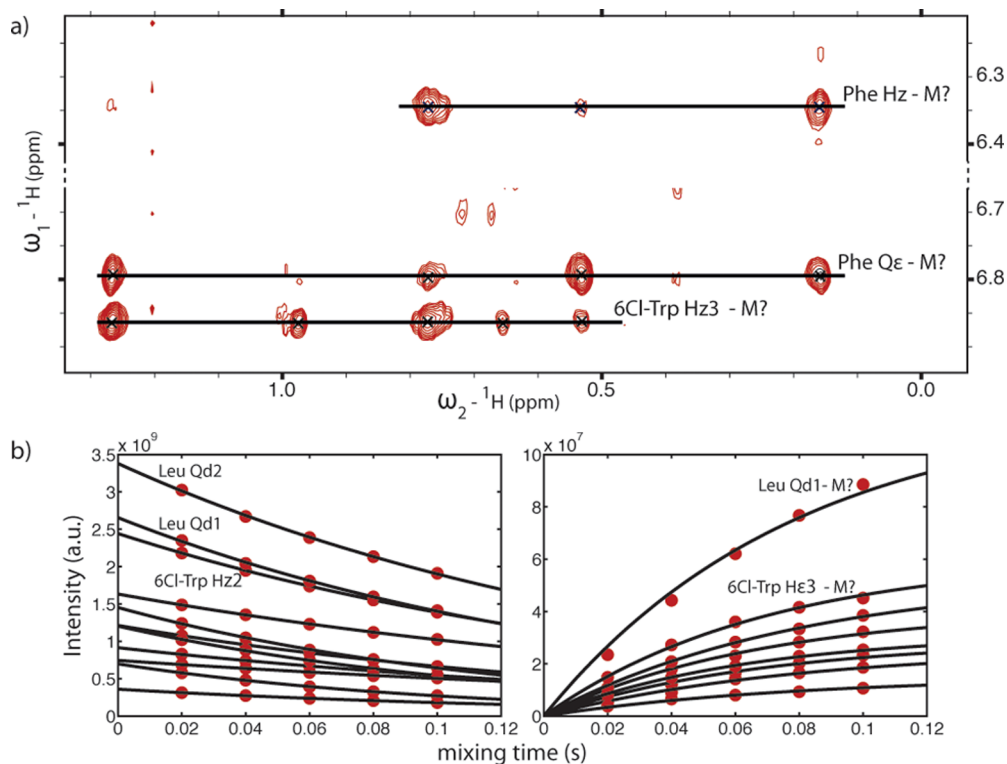


Figure 2. Experimental intermolecular NOEs of ^{15}N , ^{13}C -labeled HDMX in complex with cmpd2. (a) F_1 - ^{15}N , ^{13}C -filtered 2D- ^1H - ^1H -NOESY spectrum showing intermolecular NOEs between the ligand and unknown methyl groups of HDMX. (b) Ligand ^1H magnetization autorelaxation curves (left) and intermolecular cross-peak build-up curves (right) versus the mixing time of the filtered NOESY experiments.

only in the complex with HDMX was determined in good agreement to the crystal structure (Protein Databank: 3fea; Figure S2a and Table S3).³¹ To get a clear assessment of the success of the NMR² method, the latter was used further. Second, 21 semiquantitative intermolecular distance restraints were derived from a series of NOESY experiments and the rotational correlation time of the complex (Figure 2a,b). Third, NMR² structure calculations were carried out with several distinct input structures in order to show the broad application potential of the NMR² method as well as its robustness (Table 1): (i) crystal structure of HDMX from the HDMX–cmpd2 complex, (ii) crystal structure of HDMX in complex with a different ligand cmpd1 (shown in Figure S1c), (iii) homology model derived from the crystal structure of HDM2 (53% sequence identity to HDMX) bound to a different ligand, and (iv) homology model derived from the NMR structure of HDM2 in its apo-state.

The NMR² structure calculation with the HDMX holoprotein in complex with cmpd2 as the input structure converged after 3 cycles (Table 1) and yielded a structure of the interaction site (Figure 3a) with an accuracy relative to the crystal structure of the HDMX–cmpd2 complex of 0.4 Å heavy atom root-mean-square deviation (rmsd) for the ligand after superposition of the protein. The 10 calculations with the lowest number of violations (i.e., lowest CYANA target function, Table 1) all show an accuracy below 1 Å (Table 1) and no false positives (i.e., structures with low target function but high rmsd) were observed. The robustness of the NMR² method can also be gathered from the fact that only 16 of the 21 available NOE-derived distance restraints were used while the four remaining ones were also in agreement with the NMR² calculated structures. When starting from a structure of the

holoprotein of HDMX in complex with cmpd1, the calculation converged again after 3 cycles (Figure 3b and Table 1) with an accuracy better than 1 Å (Table 1).

Next, NMR² structure calculations were started from a homology model derived from the structure of the homologous protein HDM2 in complex with a cyclic β -hairpin ligand (PDB code 2axi). NMR² yielded a structure of the HDMX–cmpd2 complex with a ligand heavy atom rmsd to the reference of 0.9 Å (Figure 3c and Table 1). Finally, the NMR structure of the apoprotein HDM2 (PDB code 1z1m) was used as the template for a homology model of HDMX. This is a highly demanding case for NMR² because the ligand-binding site is closed in the apo state and allosteric conformational changes involving helices are necessary to accommodate the ligand (Figures S3 and S4) as indicated on experimental grounds by NMR spectroscopy (Figure S5). To show the full capabilities of the method with allowing such significant structural alterations of the protein, the NMR² protocol was extended by the introduction of loop plasticity using a potential for backbone dihedral angles during all computational steps, while the helices and β -sheets were retained and constrained solely through a hydrogen-bond network. This extended version of NMR², including flexibility in loops and side chains, produced structures with an accuracy of 1.8 Å (Table 1, Figure 3d). We also calculated the NMR² structure of the complex HDMX–cmpd2 using the protein structure from the complex HDMX–cmpd1 and the NMR-derived ligand structure in its bound conformation (Figure S2a and Table S3) yielding similar results (Figure S6).

To explore the potential of NMR² to determine the structure of ligand–protein complexes with small molecules, the complex of HDM2–nutlin-3a was investigated (Figure 4). Nutlin-3a

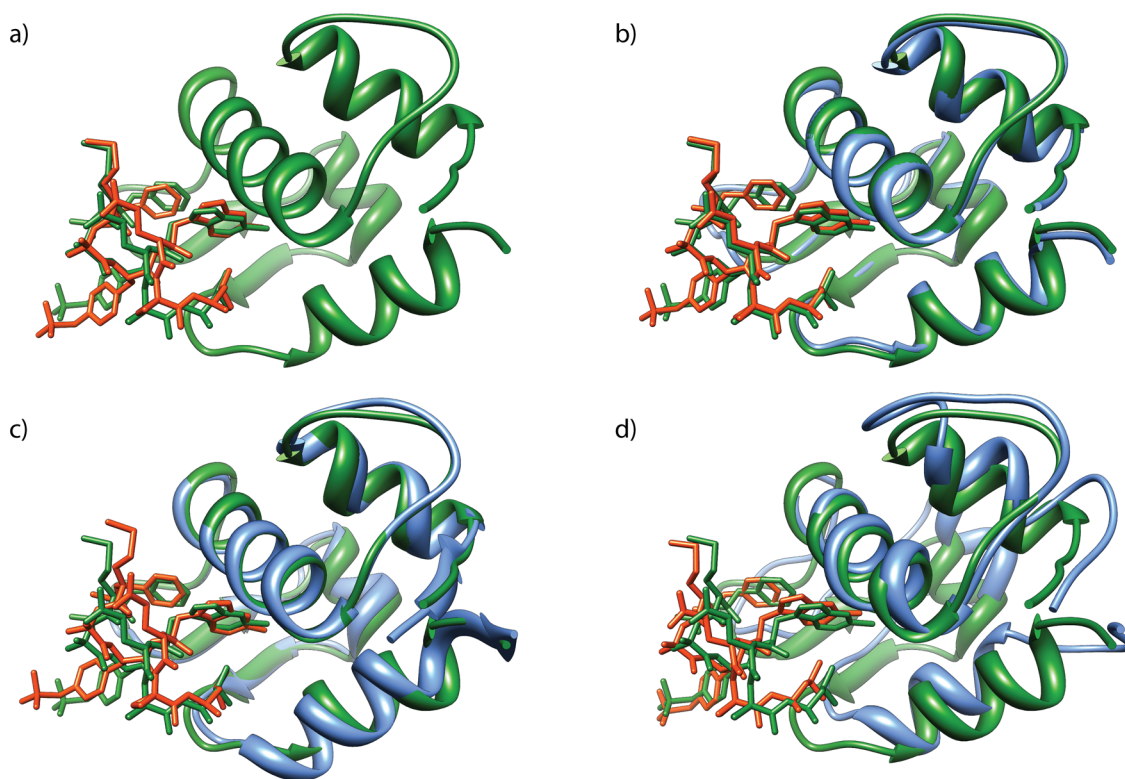


Figure 3. NMR² structures of HDMX in complex with cmpd2 under different starting scenarios using (a) the 3D structure of the native holo-protein (3fea), (b) the X-ray crystallography structure of HDMX in complex with a different ligand (3fe7), (c) a homology model of a X-ray crystallography structure of HDM2 bound to a different ligand (2axi), or (d) a homology model derived from the NMR structure of the homologous protein HDM2 (1z1m) in its ligand-free state. The reference X-ray structure of the HDMX–cmpd2 complex is colored green. The NMR²-derived structures are color-coded red for the ligand and blue for the protein with the exception of the protein structure in a because the structure is identical to the reference structure.

(Figure 5a) is a highly potent inhibitor of HDM2–p53 interaction.³² The 3D structure of this complex is also interesting because the two high-resolution X-ray crystal structures determined (PDB code 4hg7 and UniProt: Q0097, 1.9 Å resolution; PDB code 4j3e and UniProt: P56273, 1.6 Å resolution) exhibit significant differences in their nutlin-3a binding modes: The dimethyl group targeting the hydrophobic binding pocket of HDM2³³ is rotated by 80° in 4hg7 with respect to 4j3e, and overall nutlin-3a binds less deeply into the binding site (i.e., shifted by ~1.1 Å, Figure 4a). We employed the NMR² method on the HDM2–nutlin-3a complex using HDM2 in complex with p53 peptide (PDB code 3v3b) as the starting structure (Table 1). The superposition of the NMR²-derived structure with the two X-ray structures shows significant structural differences with 4hg7 (Figure 4b,c) that are attributed to crystal-packing artifacts because the ligand is located at the crystal interface.

To validate the NMR² structure we screened successfully for crystals, which do not have the ligand involved in crystal contacts (PDB code 5c5a, 1.3 Å resolution, Table S2). The NMR² and the newly determined X-ray structure show the same binding mode of nutlin-3a to HDM2 with an rmsd of 0.9 Å (Figure 4d,b).

We furthermore carried out successfully NMR² on another HDM2 complex with a small ligand called pip1 using published conventional NOE data (Biological Magnetic Resonance Data Bank entry 18755;³⁴ Figure 6 and Table 1). This finding opens the possibility to reduce greatly the time required for data

acquisition because only one mixing time was sufficient for this example.

To explore the principle versatility of NMR² to larger systems, the human ABL kinase–dasatinib complex was explored in silico (Figure S7). From the X-ray complex structure (PDB code 2gqg), the 3D structure of the ligand and intermolecular distance restraints up to 5 Å were extracted. NMR² calculations yielded the structure of the pharmacophore in the binding pocket with an accuracy of 0.9 Å (Figure S8 and Table 1).

CONCLUSIONS

It has been demonstrated on eight examples that NMR² is a fast and robust method for the determination of the 3D structure of the ligand and ligand-binding pocket at atomic resolution in solution without the requirement of protein resonances assignment. The NMR² method uses thereby a data-driven conformation search rather than a docking-scoring approach and does not require a force field as used for example by other NMR-based methods (Table S1). NMR² opens therefore an avenue for a fast establishment of structure–activity relationships of lead compounds in drug research without the need of diffracting crystals.

EXPERIMENTAL SECTION

Biochemistry. *HDMX(14–111)*. C17S (UniProt: O15151) was cloned into a pET15b (Novagen)-derived vector encoding an N-terminal His₆-tag and a HRV-3C cleavage site. Proteins were expressed in minimal medium with ¹³C-glucose and ¹⁵NH₄Cl as single sources of

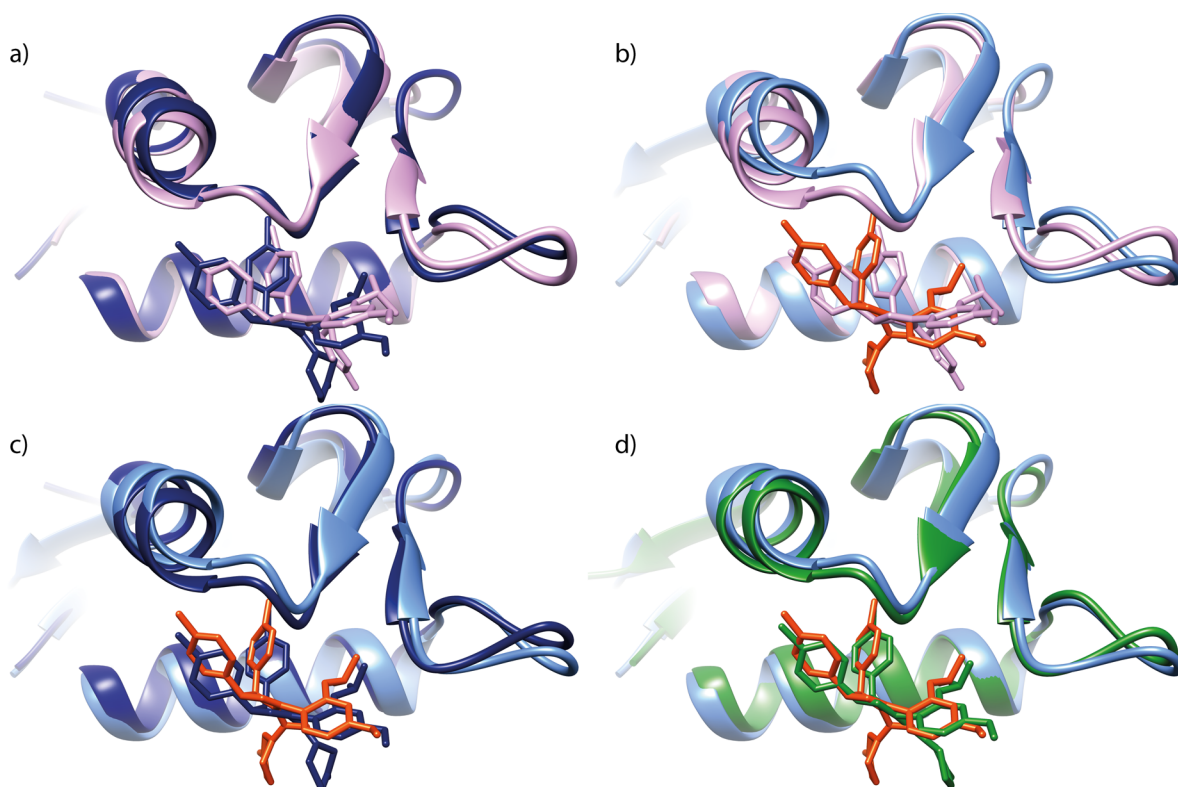


Figure 4. NMR² and X-ray structures of HDM2 in complex with the small molecule nutlin-3a. (a) Superposition of two X-ray structures of the HDM2–nutlin-3a complex. The superposition shows structural inaccuracy/inconsistency of the X-ray structures of nutlin-3a attributed to crystal packing. The HDM2 protein is represented as a pink ribbon for PDB code 4hg7 and blue for PDB code 4e3j, respectively. Nutlin-3a is represented with sticks and colored accordingly. (b) NMR² structure of HDM2 in complex with nutlin-3a is superimposed to the crystal structure with PDB code 4hg7. (c) NMR² structure of HDM2 in complex with nutlin-3a is superimposed to the crystal structure with PDB code 4e3j. The NMR²-derived structure is color-coded red for the ligand and light blue for the protein. The NMR² structure of HDM2–nutlin-3a is an accurate description of the nutlin-3a binding site as revealed by a de novo crystal-packing artifact-free structure elucidation of the HDM2–nutlin-3a complex by X-ray crystallography shown in d. This de novo X-ray structure with PDB code 5c5a is shown by a ribbon colored green for the protein and nutlin-3a with sticks and colored accordingly.

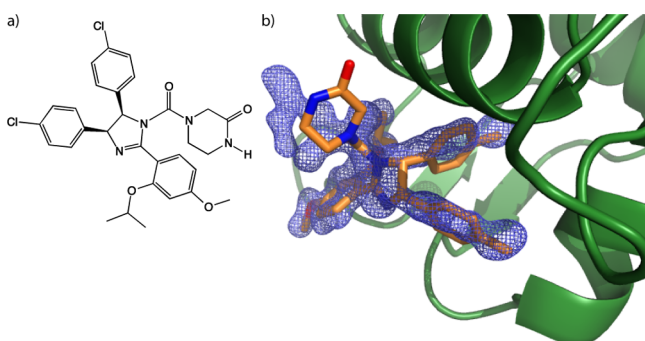


Figure 5. (a) Chemical structure of nutlin-3a. (b) Superposition of the NMR² and the artifact free X-ray structures of HDM2 in complex with nutlin-3a using the 3D structure of the p53-peptide–HDM2 complex (3v3b) as starting model. The reference X-ray structure electron density of the HDM2 nutlin-3a complex is colored blue, and the ribbons are colored green. The NMR²-derived structures are colored orange for the ligand. Sticks representation of nutlin-3a follows the atom colors red for oxygen, blue for nitrogen, and orange for carbons.

carbon and nitrogen, respectively, in 1.5 l fermenters (Labfors 4, Infors) typically yielding 15 g of wet cell mass. Cells were resuspended in 10 mL of lysis buffer per 1 g of cell pellet (lysis buffer: 50 mM Tris pH 8, 300 mM sodium chloride (NaCl), 10% glycerol, 25 mM imidazole, 2 mM tris(2-carboxyethyl)phosphine (TCEP), 0.05%

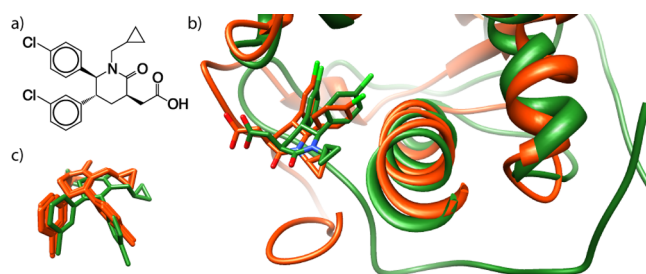


Figure 6. 3D structure of the protein–ligand complex of HDM2–pip1. (a) Chemical structure of [(3*R*,5*R*,6*S*)-5-(3-chlorophenyl)-6-(4-chlorophenyl)-1-(cyclopropylmethyl)-2-oxopiperidin-3-yl]acetic acid denoted pip1. (b) Structural superposition of the NMR²-derived ligand structure in red and the crystal structure of the HDM2–pip1 complex (PDB: 2lzg) in green.³⁴ The rmsd of the predicted ligand with respect to the reference pip1 is 1.5 Å rmsd, and the twentieth-ranked ligand prediction still exhibits a rmsd of 1.5 Å. Because the NMR protein sequence was 9 residues longer than the crystal structure used for NMR², full flexibility was applied to the angles for these residues in the NMR² calculation. (c) Best 20 NMR² conformers of pip1 with the lowest CYANA target functions. The smallest number of violations are shown in red and superimposed to pip1 in the reference HDM2–pip1 complex structure (PDB: 2lzg).

Tween 20, pH 8.0, 1 tablet/50 mL of complete, ethylenediamine-tetraacetic acid (EDTA)-free protease inhibitor, (Roche). Cells were lysed by two runs through a microfluidizer and lysates were cleared by

centrifugation at 20 000 g for 1 h at 4 °C (Sorval RC6 plus with SS34 rotor) and subsequent filtration. Proteins were captured on a self-packed 12 mL Ni-NTA superflow column (GE Healthcare), washed (50 mM Tris, 300 mM NaCl, 10% glycerol, 25 mM imidazole, 2 mM TCEP, pH 8) and eluted with a gradient to the elution buffer (50 mM Tris, 150 mM NaCl, 10% glycerol, 500 mM imidazole, 2 mM TCEP, pH 8). The His₆-tag was cleaved with HRV-3C protease (from our laboratory) overnight at 4 °C. The sample was concentrated using a 5 kDa cutoff filter and applied to a HiLoad Superdex 75 column (GE Healthcare), which was run at 10 °C (Buffer: 50 mM Tris, 200 mM NaCl, 1 mM TCEP, 1 mM EDTA, 10% glycerol, pH 7.5). Pure HDMX fractions were buffer-exchanged using a PD-10 column (GE Healthcare) to the NMR buffer (97% H₂O, 3% D₂O, 20 mM NaPi, 25 mM NaCl, with 2 mM TCEP, and 0.1 mM EDTA, at pH 7) and concentrated with a 3 kDa cutoff Amicon filter together with the ligand.

HDM2(15–111). The sequence 15–111 was cloned into a pET15v-derived vector (Novagen), containing a His₆-tag and a cleavage site, which is recognized by 3C-protease (precision protease). The expression and purification protocol was obtained from Kallen and co-workers and optimized.³¹ The construct was transformed in BL21(DE3)*, first in 2 mL of LB at 37 °C, 180 rpm, for 2–4 h and further divided into precultures of 100 mL using standard minimal media overnight at 37 °C and distributed into 1 L of minimal media. The expression was induced with 0.4 mM isopropyl- β -D-thiogalactopyranosid (IPTG) at an OD₆₀₀ of 0.8. The cells were grown overnight at 18 °C and harvested with a GS3 rotor at 4 °C, 6000 rpm, for 15 min. The pellet was used for further purification or frozen with liquid N₂ and stored at –80 °C. For the purification, the cells were resuspended in 200–250 mL of lysis buffer (containing 50 mM Tris-HCl, pH 7.5, 300 mM NaCl, 10% glycerol, 25 mM imidazole, 2 mM TCEP, 0.05% Tween20) per 25 g of pellet. Complete EDTA-free tablets were added (one tablet per 50 mL) and stirred gently at 4 °C for 30 min. The cells were lysed with the microfluidizer (Microfluidics), cycles at 40 psi, with proper cooling. Further the lysate was centrifuged at 20 000 g at 4 °C for 60 min. The supernatant was filtered through a 0.45 μ m filter and then loaded on a nickel-chelate superflow 10 mL column (Quiagen) at 4 °C very slowly at 0.8 mL/min. Washing was carried out with Buffer A (containing 50 mM Tris-HCl, pH 7.5, 300 mM NaCl, 10% glycerol, 25 mM imidazole, 2 mM TCEP) with 1 mL/min and further eluted using a gradient to Buffer B (containing 50 mM Tris-HCl, pH 7.5, 150 mM NaCl, 10% glycerol, 500 mM imidazole, 2 mM TCEP). The gradient was chosen from 0 to 100% in 60 min with a speed of 2 mL/min. PreScission protease was added in a ratio of 1:100 to the protein concentration, and the cleavage was carried out overnight with gently shaking at 4 °C. The purity was controlled by mass spectrometry. The sample was concentrated down to a maximum of 13 mL using 5000 Da concentrating columns. The solution was loaded on a HiLoad Superdex 75, HR 26/60 column previously equilibrated with Buffer C (containing 50 mM Tris-HCl, pH 7.5, 200 mM NaCl, 1 mM TCEP, 1 mM EDTA, 10% glycerol) with a speed of 1 mL/min. The respective fractions were collected and concentrated with a 5000 Da concentrating column up to 5.5 mg/mL. The final yield of ¹⁵N-labeled sample was 57 mg/L and of uniformly [¹³C,¹⁵N]-labeled 13 mg/L.

The buffer was exchanged into the buffer for NMR measurements (25 mM phosphate buffer, 25 mM NaCl, 0.1 mM deuterated EDTA, 2 mM deuterated TCEP, and 7 mM dithiothreitol (DTT) at pH 6.5) with a PD-10 column (GE Healthcare). Nutlin-3a was dissolved in deuterated dimethyl sulfoxide (DMSO) and added to the protein with a final ratio of 1:1.1. The complex was concentrated to a final protein concentration of 425 μ M.

Cocrystallization of HDM2 with Nutlin-3a. Purified HDM2 was diluted to 0.1 mM with 50 mM Tris pH 7.5, 200 mM NaCl, 1 mM TCEP, 1 mM EDTA, and 10% glycerol. Nutlin-3a was dissolved in DMSO to give a 40 mM stock concentration. Nutlin-3a was added to the 0.1 mM HDM2 solution in 2-fold excess and incubated overnight at 4 °C. Subsequently, for crystallization trials the solution was concentrated to reach a final protein concentration of 1 mM. Initial crystallization screens were dispensed using a TTP Mosquito LCP

robot (TTP LabTech) using Griener Crystal Quick-X vapor diffusion plates. Drop sizes of 200 nL reservoir and 200 nL protein were used. Crystallization was obtained in the ammonium sulfate screen from Qiagen containing 0.2 M tripotassium citrate and 2.2 M ammonium sulfate. The crystal was tested using in situ X-ray diffraction at beamline X06DA at the Swiss Light Source and did diffract up to 2 Å but showed multiple overlaying diffraction patterns characteristic of polycrystalline. Next, a seed stock was made of this crystal, and microseed matrix screening was carried into another Qiagen ammonium sulfate screen.³⁵ Crystals from the new screen appeared within 2 days under a condition containing 0.2 M potassium iodide and 2.2 M ammonium sulfate and were first tested using in situ X-ray diffraction, which confirmed that they were protein crystals with a singular diffraction pattern.

Data Collection and Structure Determination. For data collection, crystals were cryoprotected in 80% saturated lithium sulfate and flash-frozen in the cold N₂ stream. Diffraction data were collected at 100 K using the beamline X06DA of the Swiss Light Source. A total of 180° of data were collected at a wavelength of 1.0 Å with 0.1 degree oscillation and 0.1 s exposure. Data were processed using XDS³⁶ to 1.1 Å. Processing statistics are shown in Table S2. The structure was solved using molecular replacement with Phaser using the protein with PDB code 4hg7 as a model. Refinement was carried out with phenix-refine,³⁷ and model rebuilding was carried out in Coot.³⁸ Iterative rounds of model building and refinement yielded the final structure. The refinement statistics are shown in Table S2. The structure was deposited in the Protein Data Bank with accession code: 5c5a.

NMR Measurements. NMR measurements on the protein HDMX were carried out with 300 μ L of a 0.53 mM, ¹³C,¹⁵N-labeled 1:1 protein/ligand solution in the buffers described above in the “Biochemistry” section. The measurements were carried out on a Bruker 700 MHz ¹H frequency spectrometer equipped with a triple-resonance cryoprobe at 291 K for HDMX. A series of five 2D interleaved *t*₁-¹³C,¹⁵N sweep purged filter [¹H,¹H]-NOESY spectra²⁵ with mixing times $\tau_m = 20, 40, 60, 80,$ and 100 ms were recorded for the measurement of intermolecular NOE buildup curves (2048-*t*₂)*270(*t*₁) complex points, *t*_{1max} = 29.6 ms, *t*_{2max} = 225.3 ms, 160 scans, interscan delay 0.8 s). The NOESY spectra at 60 ms mixing time exhibit signal-to-noise ratios for the intermolecular NOE peaks ranging from 6 to 109 with a median at 34. ¹⁵N-*T*₁ and ¹⁵N-*T*_{1 ρ} experiments⁷ were carried out with 10, 30, 70, 160, 350, 700, and 1500 ms and 3, 6, 12, 20, 40, 80, 160, and 200 ms relaxation delays, respectively. Bound ligand proton resonance assignment was done with double purging filtered [¹H,¹H]-NOESY, TOCSY, and COSY experiments.

NMR measurements on the protein HDM2 were carried out with 300 μ L of a 0.425 mM ¹³C,¹⁵N-labeled 1:1 protein/ligand solution in the buffers described above in the “Biochemistry” section. The measurements were performed on a Bruker 700 MHz ¹H frequency spectrometer equipped with a triple resonance cryoprobe at 288.15 K. A series of three 2D *t*₁-¹³C,¹⁵N sweep purged filter-¹H,¹H]-NOESY spectra²⁵ with mixing times $\tau_m = 20, 40,$ and 60 ms was recorded for the measurement of intermolecular NOE buildup curves (2048-*t*₂)*298(*t*₁) complex points, *t*_{1max} = 27.6 ms, *t*_{2max} = 170.4 ms, 112 scans, interscan delay 0.8 s). The NOESY spectra at 60 ms mixing time exhibit signal-to-noise ratios for the intermolecular NOE peaks ranging from 5.5 to 30 with a median at 8. Proton resonance assignment of the bound ligand was done with double purging filtered [¹H,¹H]-NOESY and TOCSY and COSY experiments.

Data Analysis. All spectra were processed with NMRPipe³⁹ or toppsin 3.1 (Bruker). The evaluation of the spectra was carried out with ccpNMR analysis 2.3.⁴⁰ Semiquantitative distance measurements were derived from NOE build-up curves using a simple two-spin system model following the eNOE and previous formalisms (Table S4).^{17,26–28} First, autorelaxation rates, ρ_i , and initial magnetizations, $\Delta M_i(0)$, for the ligand protons were extracted using a mono-exponential decay model, $\Delta M_i(t) = \Delta M_i(0) \exp(-\rho_i t)$, whereas the autorelaxation rate of the protein methyl groups was set to the median of the experimentally derived autorelaxation rates. Second, cross-relaxation rates, σ_{ij} , were extracted following a two-spin system approximation model for the intermolecular

$$\text{NOEs}, \quad \Delta M_{ij}(t), \quad \frac{\Delta M_{ij}(t)}{\Delta M_{ij}(0)} = -\frac{\sigma_{ij}}{(\lambda_+ - \lambda_-)} (e^{-\lambda_+ t} - e^{-\lambda_- t}),$$

$$\text{where} \quad \lambda_{\pm} = \frac{\rho_1 + \rho_2}{2} \pm \sqrt{\left(\frac{\rho_1 - \rho_2}{2}\right)^2 + \sigma_{ij}^2}.$$

Finally, the distances, r_{ij} , are derived from the cross-relaxation rates, $\sigma_{ij} = \frac{b^2}{r_{ij}^6} (6J(2\omega) - J(0))$ with $J(\omega) = \frac{2}{5} \left(\frac{\tau_c}{1 + (\omega\tau_c)^2} \right)$, $b = \frac{1}{2} \frac{\mu_0}{4\pi} \hbar \gamma_H^2 \mu_0$ as the permeability of free space, \hbar as the reduced Planck constant, γ_H as the gyromagnetic ratio of the nucleus, and τ_c the rotational correlation time of the protein–ligand complex, which was obtained as 8.9 ns from the $^{15}\text{N}-T_1$ and $^{15}\text{N}-T_{1\rho}$ relaxation rates using the software TENSOR2.⁴¹

Protein Structures and Models. The PDB code of the initial structure of the HDMX–ligand is 3fea,³¹ the PDB code for the starting protein structure of HDMX bound to a ligand derivative is 3fe7,³¹ the PDB code of the protein HDM2 in complex with another ligand solved by X-ray crystallography at 1.4 Å resolution is 2axi,⁴² and the PDB code of the apo-structure of HDM2 solved by NMR is 1z1m,⁴³ where the conformer with lowest energy has been used. Every structure was cured if necessary for missing atoms. The homology modeling of HDMX from the HDM2 structures were carried out by the Swiss-Model homology modeling software.²⁹

Structure Calculation and Design Evaluation. Structure calculations were carried out by simulated annealing using torsion angle dynamics with the software CYANA.³⁰ Distance restraints were applied with equal upper and lower bounds. Each restraint was used under the triangle smoothing and eventually tetra-angle smoothing equations in order to limit the amount of structure calculations (around 0.5 million for a desktop computer). Distance restraint violations were measured by the target function, and in intermediate cycles structures were accepted if the target function value was $\leq 20 \text{ \AA}^2$ for distance restraints and $\leq 100 \text{ \AA}^2$ for repulsive van der Waals (no force field was used) violations. In the calculation with fully flexible protein conformation, intermediate structures with heavy atom rmsd $> 4 \text{ \AA}$ with respect to the apoprotein were also discarded for later cycles of calculations, and concerning the final NMR² predictions, the structures with the smallest backbone rmsd to the apo-receptor were selected as best predictions. 1500, 3000, and 5000 torsion angle dynamics steps were used, respectively, for the calculations with a rigid protein, fixed protein backbone and flexible side chain, and fully flexible protein with secondary structures restrained by H bonds and loops softly restrained by ϕ/ψ torsion angle restraints. Calculations took 1–5 s per structure and were carried out on a desktop computer with 8 cores, except for the large calculations in the fully flexible case of the apo protein structure, which were run on the Brutus cluster system of ETH (~700 cores).

■ ASSOCIATED CONTENT

Supporting Information

The Supporting Information is available free of charge on the ACS Publications website at DOI: 10.1021/jacs.5b12391.

NMR² tutorial files. (ZIP)

Figures S1–S10, Tables S1–S4, material and methods, and molecular modeling details. (PDF)

NMR² prediction data files. (ZIP)

■ AUTHOR INFORMATION

Corresponding Authors

*julien.orts@phys.chem.ethz.ch

*roland.riek@phys.chem.ethz.ch

Notes

The authors declare no competing financial interest.

■ ACKNOWLEDGMENTS

We thank V. Tundo and M. Maschlej for preparation of several protein samples and W. Jahnke for fruitful discussions. The

ETH Zürich, the FEBS (long-term fellowship to J.O.), the Lichtenberg program of the Volkswagen Foundation and the Japan Society for the Promotion of Science financially supported this work.

■ REFERENCES

- Rossmann, M. G.; Blow, D. M. *Acta Crystallogr.* **1962**, *15*, 24.
- Hillisch, A.; Pineda, L. F.; Hilgenfeld, R. *Drug Discovery Today* **2004**, *9*, 659.
- Cavanagh, J.; Fairbrother, W. J.; Palmer, A. G.; Rance, M.; Sklepton, N. J. *Protein NMR Spectroscopy, Principles and Practice*; Academic Press: San Diego, CA, 2007.
- Nilges, M. J. *Mol. Biol.* **1995**, *245*, 645.
- Nilges, M.; O'Donoghue, S. I. *Prog. Nucl. Magn. Reson. Spectrosc.* **1998**, *32*, 107.
- Dominguez, C.; Boelens, R.; Bonvin, A. M. J. J. *J. Am. Chem. Soc.* **2003**, *125*, 1731.
- Clore, G. M.; Schwieters, C. D. *J. Am. Chem. Soc.* **2003**, *125*, 2902.
- Wang, B.; Westerhoff, L. M.; Merz, K. M. *J. Med. Chem.* **2007**, *50*, 5128.
- McCoy, M. A.; Wyss, D. F. *J. Am. Chem. Soc.* **2002**, *124*, 11758.
- Cioffi, M.; Hunter, C. A.; Packer, M. J.; Spitaleri, A. J. *Med. Chem.* **2008**, *51*, 2512.
- Hajduk, P. J.; Mack, J. C.; Olejniczak, E. T.; Park, C.; Dandliker, P. J.; Beutel, B. A. *J. Am. Chem. Soc.* **2004**, *126*, 2390.
- Jayalakshmi, V.; Rama Krishna, N. J. *Magn. Reson.* **2004**, *168*, 36.
- Schieberr, U.; Vogtherr, M.; Elshorsh, B.; Betz, M.; Grimme, S.; Pescatore, B.; Langer, T.; Saxena, K.; Schwalbe, H. *ChemBioChem* **2005**, *6*, 1891.
- Orts, J.; Bartoschek, S.; Griesinger, C.; Monecke, P.; Carlomagno, T. *J. Biomol. NMR* **2012**, *52*, 23.
- Constantine, K. L.; Davis, M. E.; Metzler, W. J.; Mueller, L.; Claus, B. L. *J. Am. Chem. Soc.* **2006**, *128*, 7252.
- Orts, J.; Grimm, S. K.; Griesinger, C.; Wendt, K. U.; Bartoschek, S.; Carlomagno, T. *Chem. - Eur. J.* **2008**, *14*, 7517.
- Noggle, J. H.; Schirmer, R. E. *The Nuclear Overhauser Effect*; Academic Press: New York, 1971.
- Balaran, P.; Bothner-By, A. A.; Breslow, E. *J. Am. Chem. Soc.* **1972**, *94*, 4017.
- Kaiser, R. *J. Chem. Phys.* **1965**, *42*, 1838.
- Shvarts, A.; Steegenga, W. T.; Riteco, N.; vanLaar, T.; Dekker, P.; Bazuine, M.; vanHam, R. C. A.; vanOordt, W. V.; Hateboer, G.; vanderEb, A. J.; Jochemsen, A. G. *EMBO J.* **1996**, *15*, 5349.
- Barboza, J. A.; Iwakuma, T.; Terzian, T.; El-Naggar, A. K.; Lozano, G. *Mol. Cancer Res.* **2008**, *6*, 947.
- Breeze, A. L. *Prog. Nucl. Magn. Reson. Spectrosc.* **2000**, *36*, 323.
- Otting, G.; Wüthrich, K. *Q. Rev. Biophys.* **1990**, *23*, 39.
- Kogler, H.; Sorensen, O. W.; Bodenhausen, G.; Ernst, R. R. J. *Magn. Reson.* **1983**, *55*, 157.
- Zwahlen, C.; Legault, P.; Vincent, S. J. F.; Greenblatt, J.; Konrat, R.; Kay, L. E. *J. Am. Chem. Soc.* **1997**, *119*, 6711.
- Ni, F. *Prog. Nucl. Magn. Reson. Spectrosc.* **1994**, *26*, 517.
- Orts, J.; Vögeli, B.; Riek, R. *J. Chem. Theory Comput.* **2012**, *8*, 3483.
- Vögeli, B.; Segawa, T. F.; Leitz, D.; Sobol, A.; Choutko, A.; Trzesniak, D.; van Gunsteren, W.; Riek, R. *J. Am. Chem. Soc.* **2009**, *131*, 17215.
- Schwede, T.; Kopp, J.; Guex, N.; Peitsch, M. C. *Nucleic Acids Res.* **2003**, *31*, 3381.
- Güntert, P.; Mumenthaler, C.; Wüthrich, K. *J. Mol. Biol.* **1997**, *273*, 283.
- Kallen, J.; Goepfert, A.; Blechschmidt, A.; Izaac, A.; Geiser, M.; Tavares, G.; Ramage, P.; Furet, P.; Masuya, K.; Lisztwan, J. *J. Biol. Chem.* **2009**, *284*, 8812.
- Vassilev, L. T.; Vu, B. T.; Graves, B.; Carvajal, D.; Podlaski, F.; Filipovic, Z.; Kong, N.; Kammlott, U.; Lukacs, C.; Klein, C.; Fotouhi, N.; Liu, E. A. *Science* **2004**, *303*, 844.

- (33) Kussie, P. H.; Gorina, S.; Marechal, V.; Elenbaas, B.; Moreau, J.; Levine, A. J.; Pavletich, N. P. *Science* **1996**, *274*, 948.
- (34) Michelsen, K.; Jordan, J. B.; Lewis, J.; Long, A. M.; Yang, E.; Rew, Y.; Zhou, J.; Yakowec, P.; Schnier, P. D.; Huang, X.; Poppe, L. J. *Am. Chem. Soc.* **2012**, *134*, 17059.
- (35) D'arcy, A.; Bergfors, T.; Cowan-Jacob, S. W.; Marsh, M. *Acta Crystallogr., Sect. F: Struct. Biol. Commun.* **2014**, *70*, 1117.
- (36) Kabsch, W. *Acta Crystallogr., Sect. D: Biol. Crystallogr.* **2010**, *66*, 125.
- (37) Afonine, P. V.; Grosse-Kunstleve, R. W.; Adams, P. D. *Acta Crystallogr., Sect. D: Biol. Crystallogr.* **2005**, *61*, 850.
- (38) Emsley, P.; Lohkamp, B.; Scott, W. G.; Cowtan, K. *Acta Crystallogr., Sect. D: Biol. Crystallogr.* **2010**, *66*, 486.
- (39) Delaglio, F.; Grzesiek, S.; Vuister, G. W.; Zhu, G.; Pfeifer, J.; Bax, A. *J. Biomol. NMR* **1995**, *6*, 277.
- (40) Vranken, W. F.; Boucher, W.; Stevens, T. J.; Fogh, R. H.; Pajon, A.; Llinas, P.; Ulrich, E. L.; Markley, J. L.; Ionides, J.; Laue, E. D. *Proteins: Struct., Funct., Genet.* **2005**, *59*, 687.
- (41) Blackledge, M.; Cordier, F.; Dosset, P.; Marion, D. *J. Am. Chem. Soc.* **1998**, *120*, 4538.
- (42) Fasan, R.; Dias, R. L. A.; Moehle, K.; Zerbe, O.; Obrecht, D.; Mittl, P. R. E.; Grutter, M. G.; Robinson, J. A. *ChemBioChem* **2006**, *7*, 515.
- (43) Uhrinova, S.; Uhrin, D.; Powers, H.; Watt, K.; Zheleva, D.; Fischer, P.; McInnes, C.; Barlow, P. N. *J. Mol. Biol.* **2005**, *350*, 587.